

N87-11209

HIGH TEMPERATURE STRESS-STRAIN ANALYSIS

Robert L. Thompson
National Aeronautics and Space Administration
Lewis Research Center

INTRODUCTION

The objectives of the HOST Burner Liner Cyclic Rig Program are threefold: (1) to assist in developing predictive tools needed to improve design analyses and procedures for the efficient and accurate prediction of burner liner structural performance and response; (2) to calibrate, validate, and evaluate these predictive tools by comparing the predicted results with the experimental data; and (3) to evaluate existing as well as advanced temperature and strain measurement instrumentation, through both contact and noncontact efforts, in a simulated turbine engine combustor environment. As the predictive tools, as well as the tests, test methods, instrumentation, and data acquisition and reduction methods are developed and evaluated, a proven, integrated analysis/experiment method will be developed that will permit the accurate prediction of the cyclic life of a burner liner.

TEST RIGS

The above objectives will be partially accomplished with two experimental rigs, one a bench-top rig to test 8- by 5-in flat plates under thermal cycling conditions and the other an annular rig to test 20-inch diameter cylindrical test specimens. Figure 1 shows the major components and the installation of the bench-top rig which is about 90 percent complete. Four quartz lamps (6 kW each) are used to heat the plate specimens. Water and/or air cooling are used to cool the fixture, lamps, and test plate. Cooling air to the plate can be preheated. A viewing port provides for visual inspection of the plate and data acquisition with an infrared (IR) camera system. Provisions for instrumentation include 30 thermocouples and 10 strain gauges.

Figure 2 shows the annular rig installation which is about 75 percent complete. Shown also is the stacked-ring louver burner liner to be tested first. Simpler liners as well as advanced liners will also be tested, primarily deformation testing and some fatigue testing will be done. The quartz lamp heating system supplied by Research, Inc., under contract to Pratt & Whitney Aircraft (P&WA) is shown in figure 3. This rig and program are a cooperative effort between NASA Lewis and P&WA. P&WA supplied the test section, which includes the heating system, and is supplying technical assistance to the program. NASA Lewis is providing the test facility and operators and other technical expertise. The heat source is 112 quartz lamps (6 kW each) configured circumferentially in 16 sectors each having 7 lamps. Water and/or air are used to cool the fixture, lamps, and test specimen. Cooling air to the specimen can be preheated. A natural gas and air mixture will be burned to preheat the air to about 500 °F. Cooled viewing ports are provided for visual inspection of the specimen, and thermal data acquisition with an infrared system. Seven quick-disconnect instrumentation panels provide for 99 thermocouples, 28 strain gauges, and 21 pressure transducer connections.

TESTS

To verify the feasibility of the test and the bench-top rig design and to identify potential test problems and analysis/experimental complications, a limited number of steady-state and transient tests were conducted. Structural analyses were performed on the 5- by 8- by 0.05-in Hastelloy-X flat plate specimen tested. Figure 4 shows the steady-state temperatures of the Hastelloy-X plate heated at various power levels for three cooling airflows to the plate. The maximum plate temperature is plotted as a function of the applied power level. The cooling air to the plate was varied in steps from 0 to 0.05 to 0.1 lb/sec. The solid points show the effect of preheating the cooling air to the plate to about 430 °F. Note that a 60 percent power level results in a maximum plate temperature of about 1800 °F (maximum normal temperature of a Hastelloy-X combustor liner), while cooling the plate reduces the maximum temperature of the plate appreciably.

Figures 5 to 7 show the cold-side steady-state plate temperatures. Seven thermocouples are used to measure plate temperature. Their locations are shown in the sketch in figure 5. Steady-state temperatures are plotted as functions of the plate centerline temperatures in the horizontal and vertical directions for several applied power levels. With no plate cooling (fig. 5), the heating of the plate for the four power levels is nonuniform, with the lower right quadrant of the plate being much cooler than the others. This is attributed to uneven plate oxidation, the different lamps used, and cooling shelf on which the specimen rests. Figures 6 and 7 show the effect of cooling air on the plate temperatures. These curves show that the axial temperature distribution on the plate can be controlled by varying the cooling airflow. Hot-side plate temperatures were also measured. Through the thickness temperature gradients of 20 to 30 F° were obtained.

Some results of thermal cycling of a test plate are shown in figures 8 and 9. The power was varied cyclically from 5 to 100 percent and back down to 5 percent with a 148/sec cycle time as shown in figure 8(a). The maximum plate temperature for this cycle is shown in figure 8(b). Cooling air flow to the plate was at its maximum at 0.1 lb/sec. The preheater was used to preheat the cooling air to the plate to about 430 °F. Figure 9 shows the maximum temperature of the plate as a function of the number of thermal cycles. The minimum temperature at 5 percent power is also shown for the same location. After the first thermal cycle the temperatures were very repeatable. A specified temperature history can also be run, in which case the power is the dependent variable. No data are shown for this case. A programmable microprocessor is used to run the tests in either the power control mode or the temperature control mode.

Cold-side plate temperatures are measured with both thermocouples and a computer-controlled infrared camera system. The major components of the IR system are shown in figure 10. Typical calibration curves for the system are shown in figure 11 where intensity is plotted against thermocouple temperature. Curves like these are used to obtain temperatures from a thermal image and also to determine the emissivity of Hastelloy-X plates. The emissivity of Hastelloy-X was determined to be about 0.88 to 0.90 and was not found to be a function of temperature.

Thermal images of the plate, viewed through the quartz window, for a typical thermal cycle are shown in figure 12. The thermal images obtained from the tests are recorded on a VHS tape recorder, with an image recorded every 1/30 of a second. The thermal images recorded are processed and analyzed following the test using the computer. The processed temperature data are then saved on a magnetic tape for further processing and analysis on the Lewis IBM 370 mainframe computer. This

capability has not been fully demonstrated. The capability also exists to monitor in real time the plate temperature at any point within the field of view of the IR camera. Another use of the IR system is as a diagnostic tool.

Figures 13 and 14 show a comparison of the infrared data with thermocouple data. The thermocouple data and other research and facilities data are acquired with the ESCORT II data acquisition system and stored on the mainframe computer. Steady-state temperatures are compared in figure 13 for a 90 percent power level with cooling air to the plate. There is good agreement between the thermocouple and infrared temperature data, with the maximum difference being about 5 percent. Figure 14 shows a comparison of IR data with thermocouple data for a thermal cycle. Figure 15 illustrates a temperature distribution of the plate obtained from the IR and thermocouple data, to be saved for further analysis.

The experience gained from the bench-top rig operation is and will be carried over to the annular rig. For example, a noncontact strain measurement device will be tested on the bench-top rig. If it is successful, it will be used on the annular rig. Also, lamp durability tests are underway on the bench-top rig. The data and information obtained from these tests will be applied to the annular rig.

The installation of the annular rig is nearing completion. An evaluation of the vitiated preheater for the annular rig has been completed. Air and natural gas were burned in a modified GE J-47 combustor can. Performance results of these tests were the average exit air temperature varied from 400 to 600 °F (500 °F was the nominal design temperature); the pattern factor ranged from 0.009 to 0.053; air-flow rate was varied from 3.5 to 8.0 lb/sec (design conditions); the maximum liner temperature was 700 °F; and no smoke or soot was emitted. The heating system is being installed. Checkout of the water coolant system for the heater is scheduled for October 1984 and checkout of the complete rig is set for November. Testing of the stacked-ring louver liner could begin in December with the testing of simpler as well as advanced liners to follow.

ANALYSIS

The objectives of this program will be partially accomplished with the structural analysis of specimens. A structural analysis of a flat-plate specimen was performed using MARC, a general purpose nonlinear finite-element structural analysis program. The Walker, the Miller, and the Krieg, Swearngen, and Rhode (KSR) viscoplastic constitutive models have been incorporated into MARC. These models can account for the interaction between creep and plastic deformations and strain-rate effects, among others, critical to a burner liner design.

The plate was analyzed using a four-node plane stress element. The mesh configuration is shown in figure 16. The configuration is doubly symmetric and thus only a quarter of the plate is modelled. The finite-element model of frame and plate is also shown where the frame is modelled with bar elements.

For the structural analysis, uniform temperatures were assumed for the plate and frame, with about a 20-percent temperature difference between the plate and frame as shown in figure 17. The maximum principal strains in the plate for the assumed temperature history are shown in figure 18 for the three viscoplastic models. The comparison shows no difference in the prediction of the strains. However, a comparison of the maximum stress component S_x for the three viscoplastic models shows considerable differences (fig. 19). The Miller and KSR models give similar

stresses, while the Walker model gives higher stresses. Figure 20 shows hysteresis loops (maximum stress versus strain) for the three viscoplastic models. No direct comparisons have yet been made between the analysis and experiment because of the nonuniformity of plate temperatures obtained from experiments. However, the structural analysis of plates with nonuniform temperatures obtained from experimental data is underway. Also underway are structural analyses of two-dimensional axisymmetric and three-dimensional burner liner models.

SUMMARY

The preliminary tests conducted with the bench-top rig have demonstrated that the desired plate temperatures, temperature gradient (through the thickness and axially), and repeatable temperature histories can be achieved, although near uniform plate temperatures have yet to be achieved. Finite-element models of plates have been generated and structural analyses of these plates with uniform plate temperatures have been performed using three viscoplastic models. Structural analysis of plates with nonuniform temperatures is underway as are two- and three-dimensional analyses of burner liners.

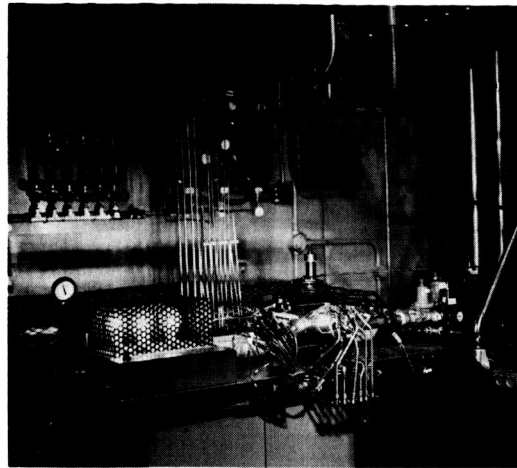
It has been demonstrated on the bench-top rig that the temperature data obtained from the thermocouples can be collected with the ESCORT II data acquisition system and that these data can then be stored on the Lewis IBM 370 computer for further processing, reduction, and analysis. It has also been demonstrated that the IR camera system can provide accurate temperature maps of the flat plate and can also be used as a diagnostic tool. The system to transfer thermal information from the IR system to the mainframe is in place but has not been demonstrated fully. The experience gained from the bench-top rig installation and operation is being carried over to the annular rig.

The annular rig installation is nearing completion and will provide data on cylindrical tubes and subelements of burner liners. Tests run with the vitiated preheater on the Annular rig were successful.

Structural analyses will be performed to predict the material stress-strain response of plates and burner liners using measured temperature distributions. These analyses will provide a basis for comparing analytical predictions, for example, using several viscoplastic constitutive models, with experimental data for validation and subsequent selection of improved analysis methods to predict accurate and efficient structural responses of burner liners.

BENCH TOP QUARTZ LAMP FLAT PLATE TEST RIG

- QUARTZ LAMPS
- AIR LINES
- WATER LINES
- IR CAMERA

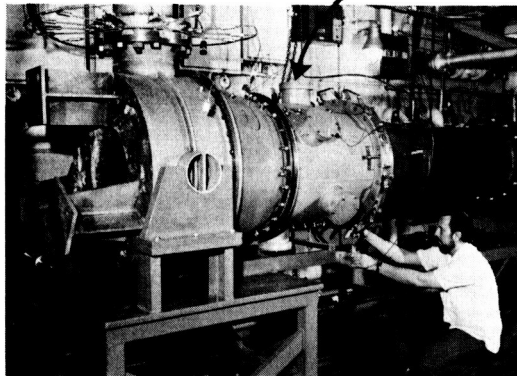


- VIEWING PORT
AND COVER
- DIFFUSOR PLATE
- LAMP-OUT DETECTION
SYSTEM

CS 84-3985

Figure 1

ANNULAR QUARTZ LAMP COMBUSTOR TEST RIG



STACKED RING LOUVER LINER

CS 84-3984

Figure 2

QUARTZ LAMP CYCLIC COMBUSTOR TEST RIG SCHEMATIC

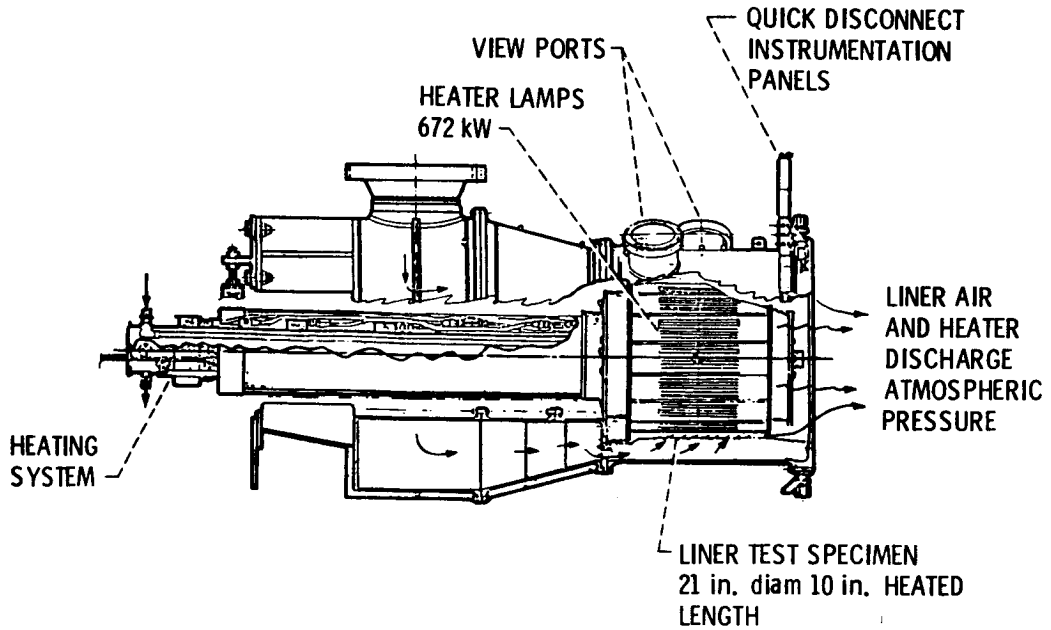


Figure 3

HASTELLOY-X FLAT PLATE HEATED TO STEADY-STATE CONDITIONS

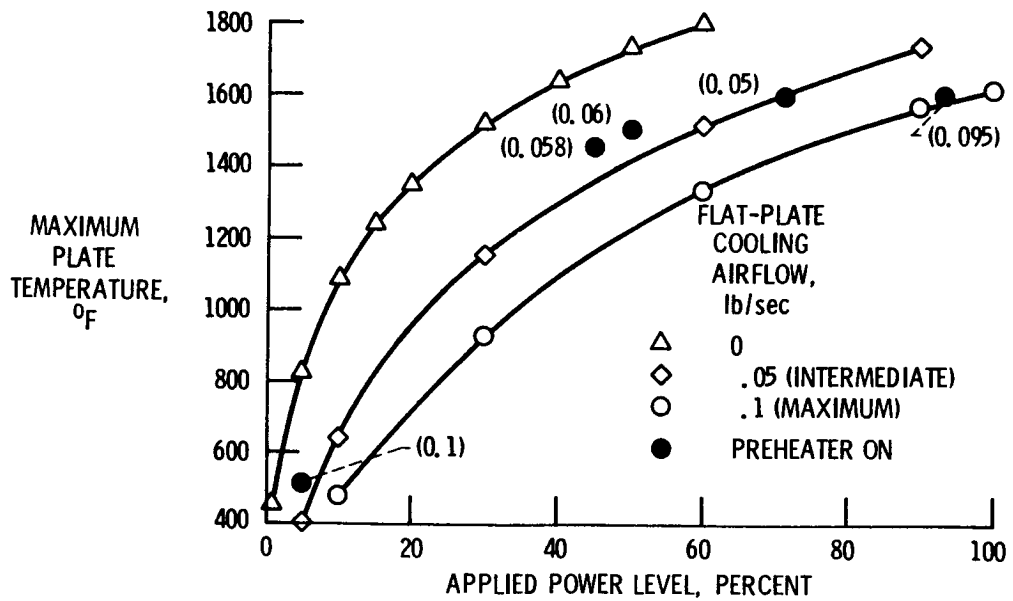


Figure 4

COLD-SIDE PLATE TEMPERATURES FOR NO PLATE COOLING

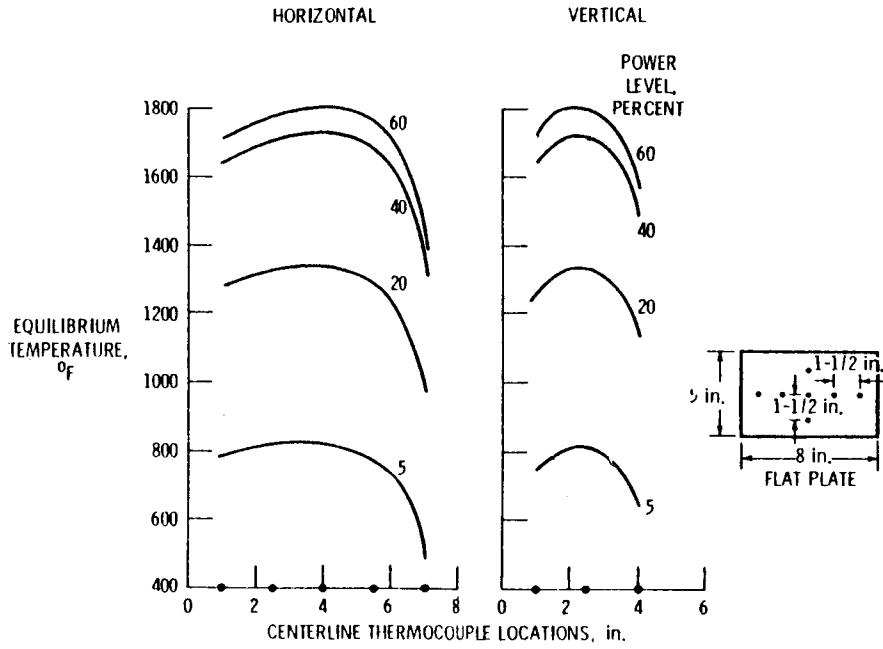


Figure 5

COLD-SIDE PLATE TEMPERATURES FOR INTERMEDIATE PLATE COOLING

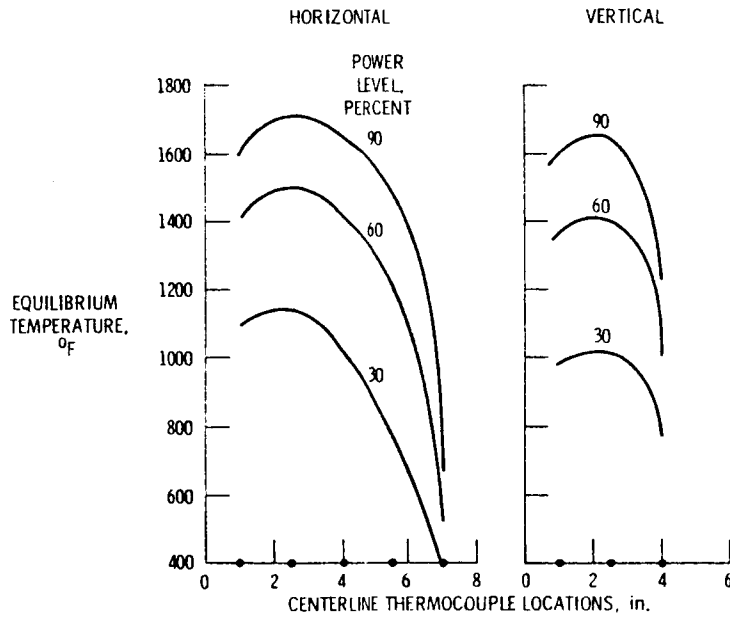


Figure 6

COLD-SIDE PLATE TEMPERATURES FOR MAXIMUM PLATE COOLING

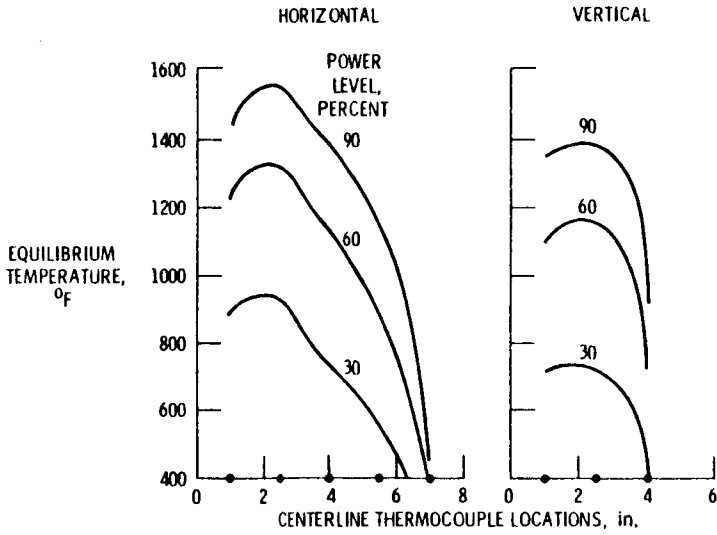


Figure 7

THERMAL CYCLING OF FLAT PLATE

MAXIMUM PLATE TEMPERATURE RESULTING FROM APPLIED POWER HISTORY

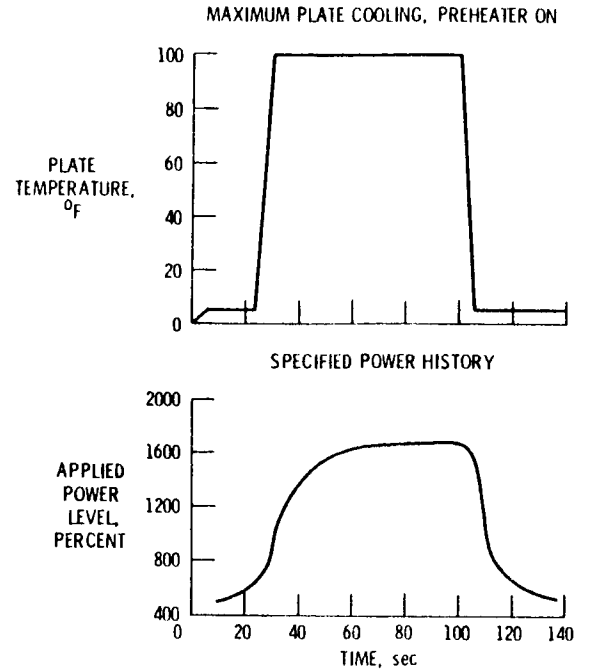


Figure 8

CYCLIC HEATING OF TEST PLATE

MAXIMUM PLATE COOLING; PREHEATER ON

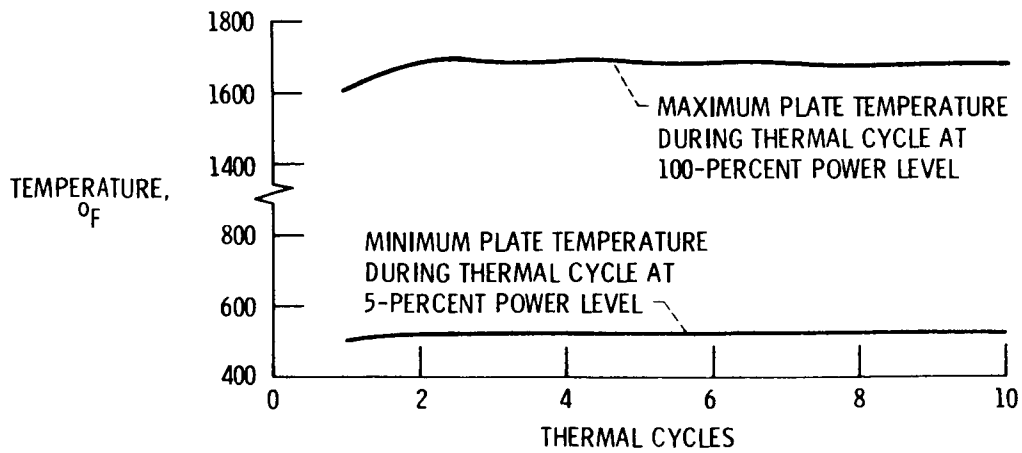


Figure 9

INFRARED THERMOVISION SYSTEM INSTALLATION

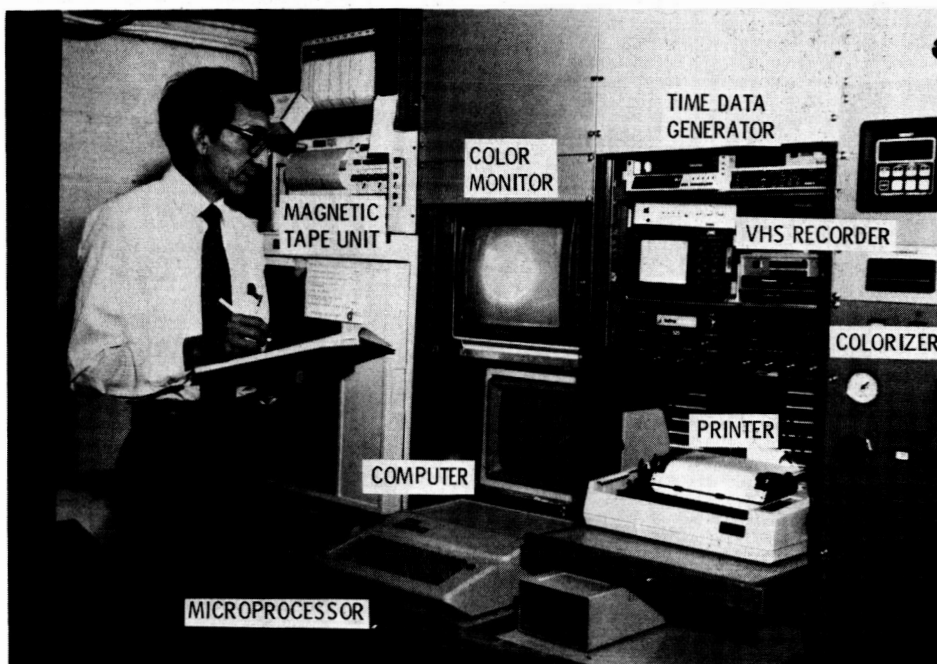


Figure 10

CS 84-3983

CALIBRATION CURVES FOR INFRARED CAMERA

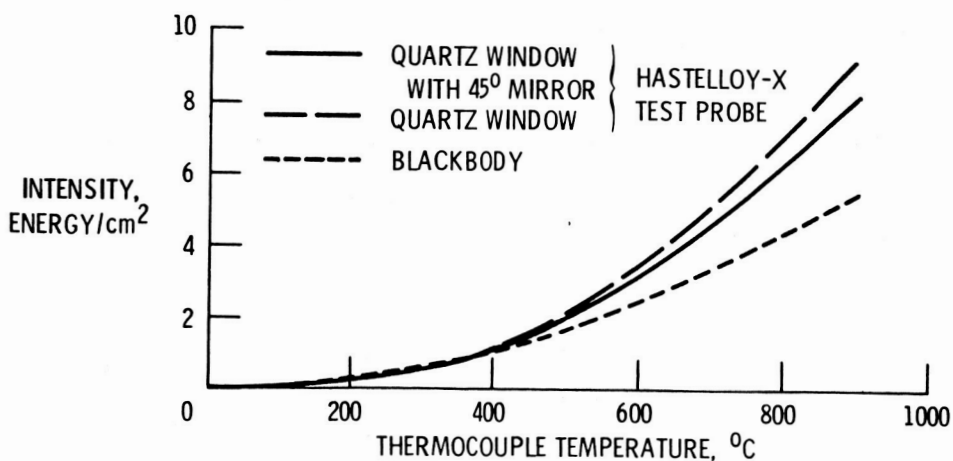
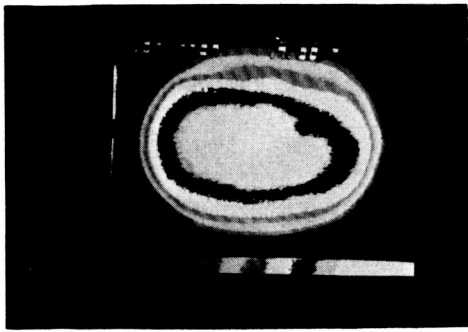
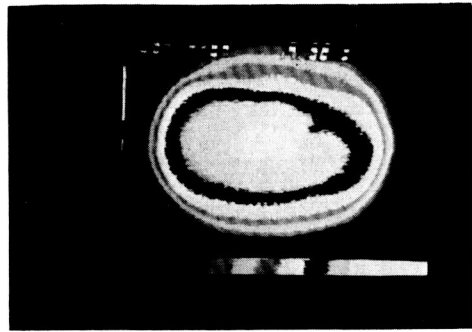


Figure 11

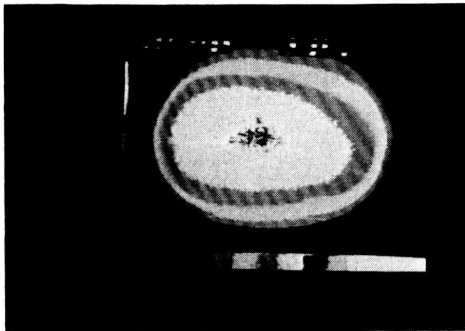
THERMAL IMAGES OF HASTELLOY-X PLATE FOR TYPICAL THERMAL CYCLE



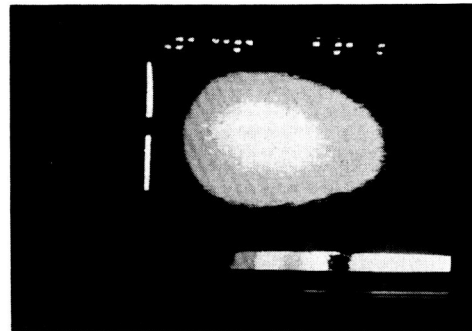
50 sec



60 sec

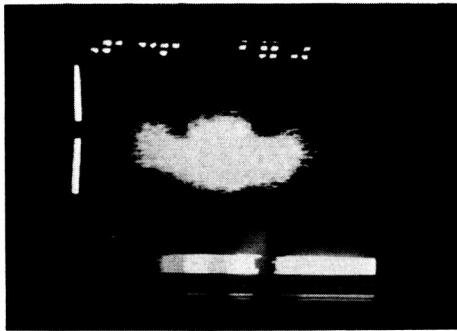


70 sec

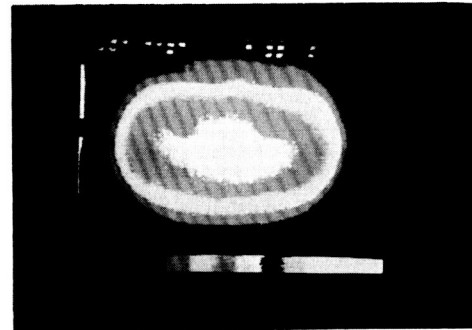


80 sec

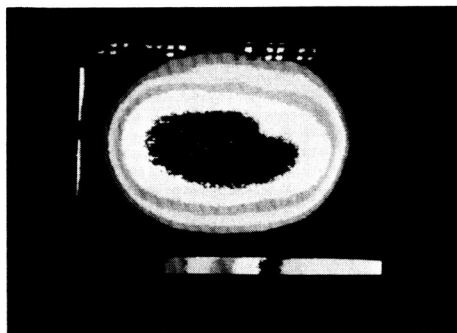
CS 84-3986



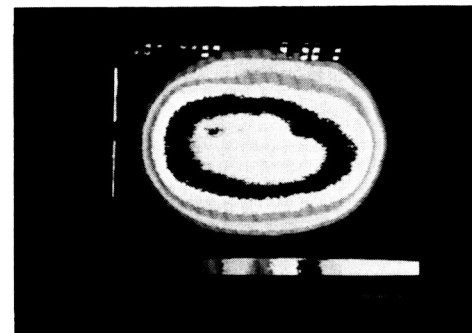
0 sec



20 sec



30 sec



40 sec

CS 84-3987

Figure 12

STEADY-STATE COMPARISON OF IR CAMERA AND THERMOCOUPLE DATA

90-PERCENT POWER LEVEL COOLED PLATE

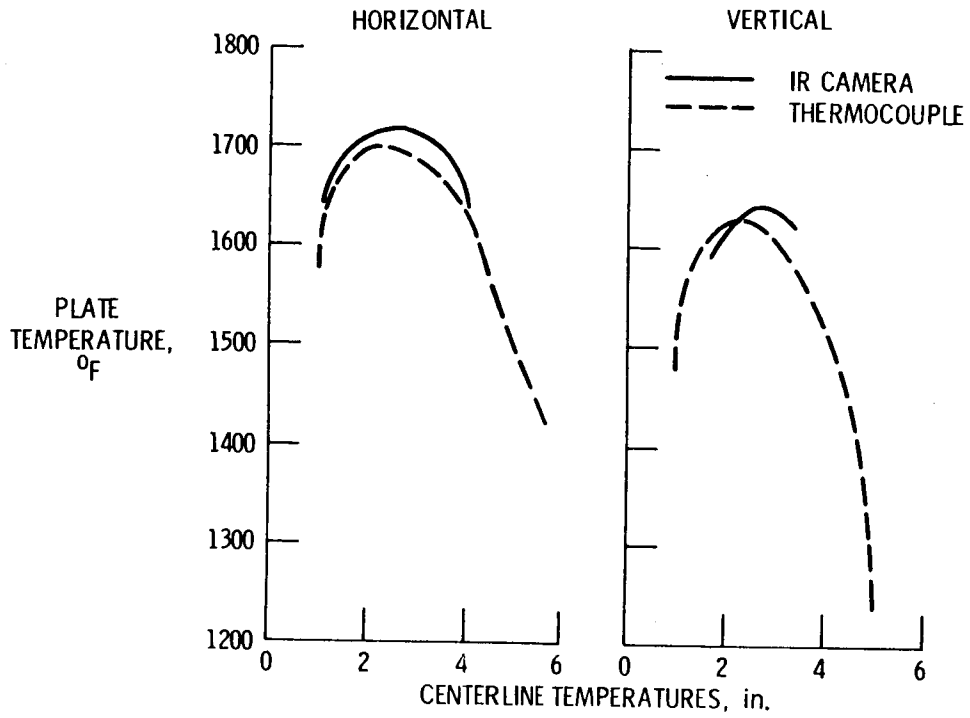


Figure 13

COMPARISON OF IR CAMERA AND THERMOCOUPLE DATA FOR ONE THERMAL CYCLE

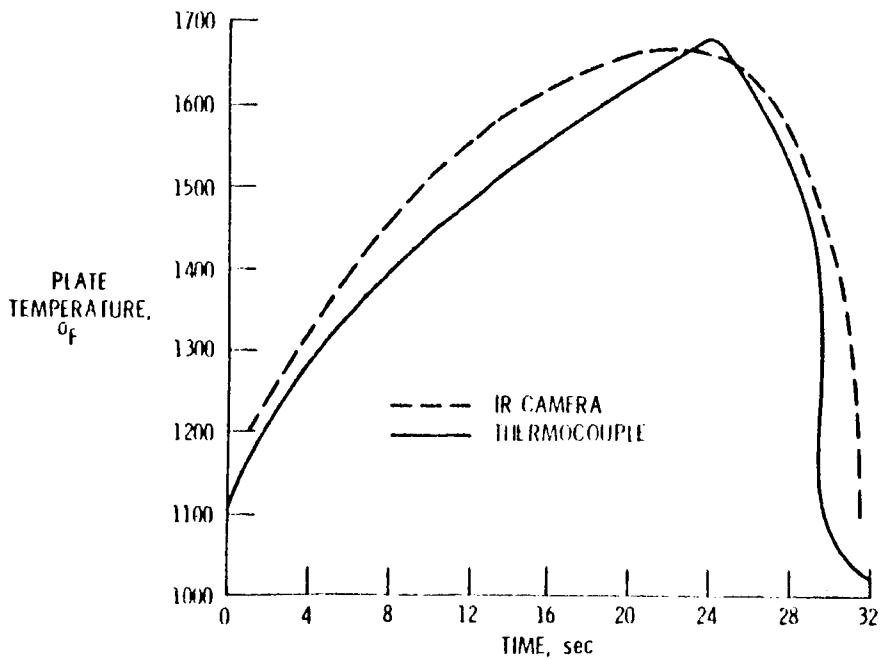


Figure 14

REPRESENTATIVE TEMPERATURE DISTRIBUTION ON 8 x 5 in. FLAT PLATE

60-PERCENT POWER; NO PLATE COOLING

1500	1520	1590	1610	1600	1570	1510	1410
1510	1530	1640	1640	1620	1590	1530	1430
1520	1560	1670	1670	1650	1610	1550	1450
1560	1610	1720	1700	1690	1650	1520	1420
1530	1580	1690	1670	1660	1600	1500	1400
1520	1550	1640	1640	1640	1560	1480	1390

Figure 15

FINITE-ELEMENT MODELS

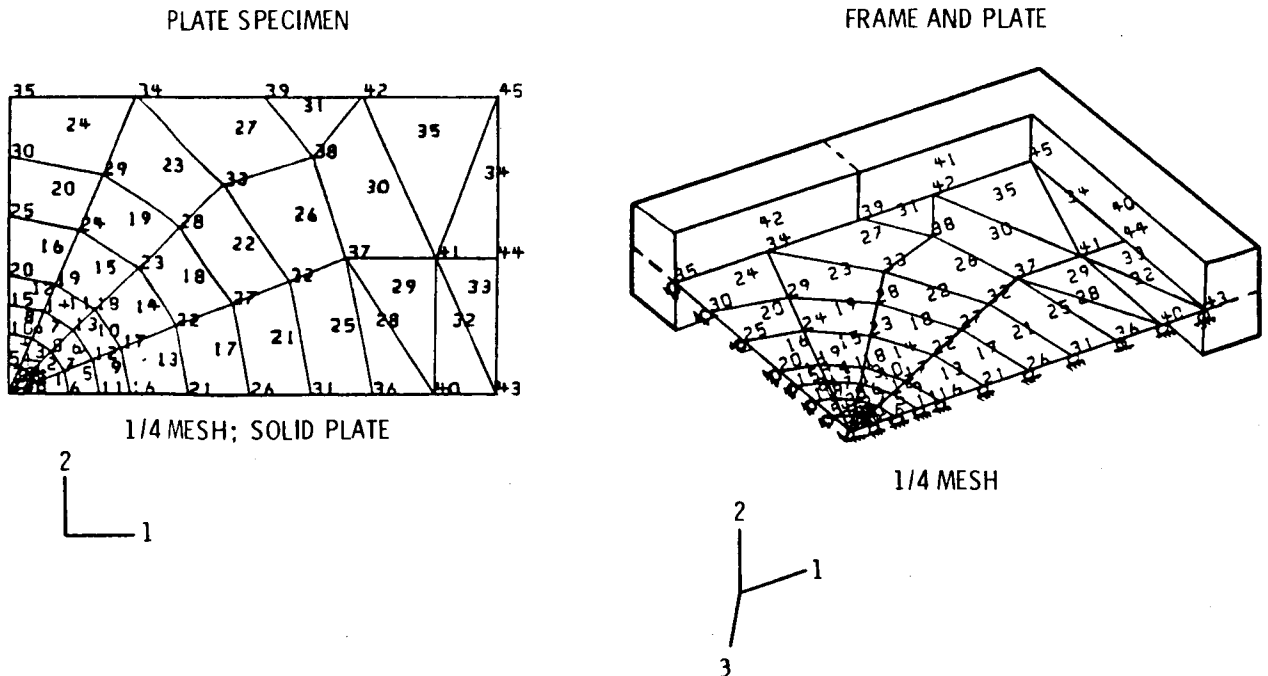


Figure 16

UNIFORM TEMPERATURE HISTORY OF PLATE AND FRAME

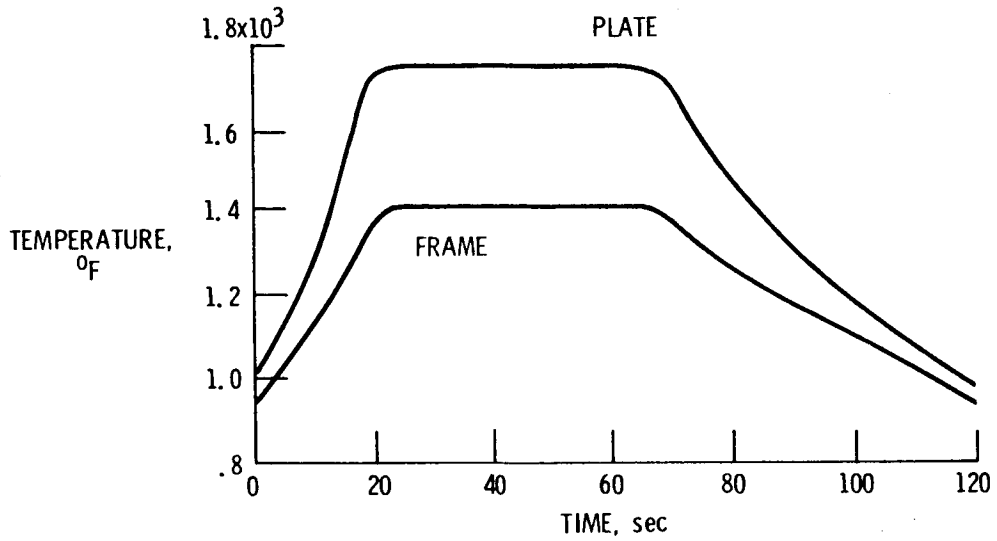


Figure 17

COMPARISON OF THREE VISCOPLASTIC THEORIES

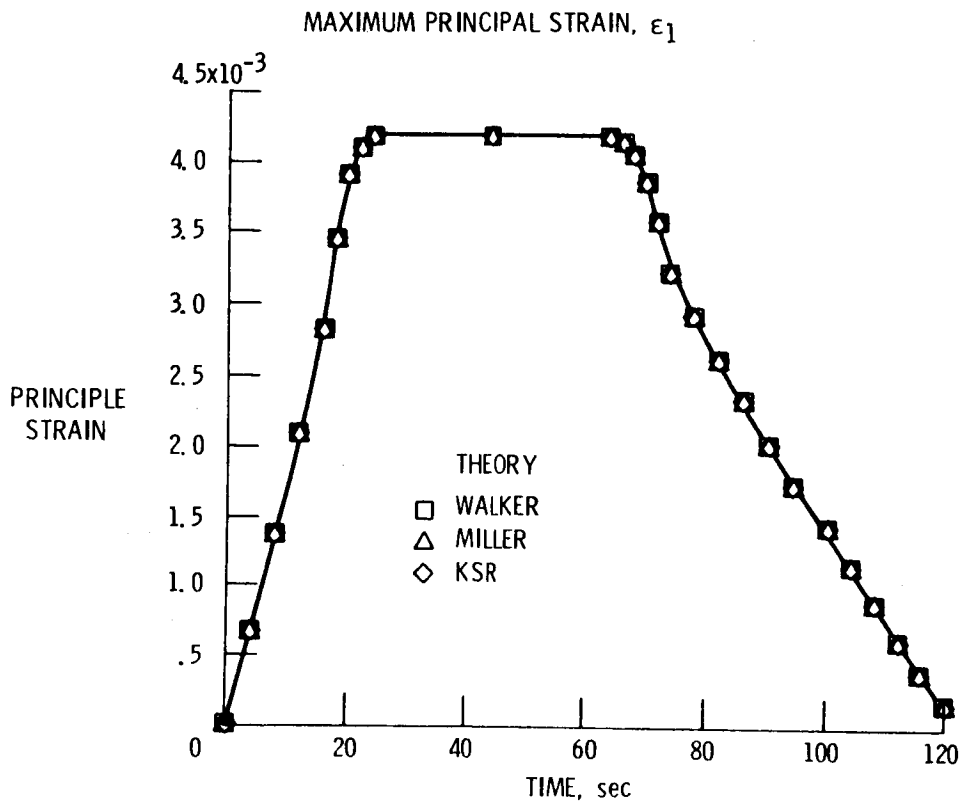


Figure 18

COMPARISON OF THREE VISCOPLASTIC THEORIES

STRESS COMPONENT, S_x

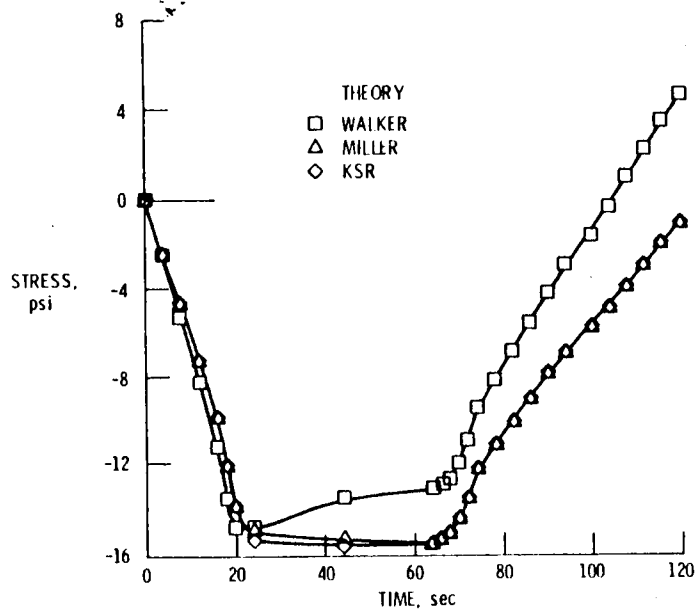


Figure 19

COMPARISON OF THREE VISCOPLASTIC THEORIES

HYSTERESIS LOOPS

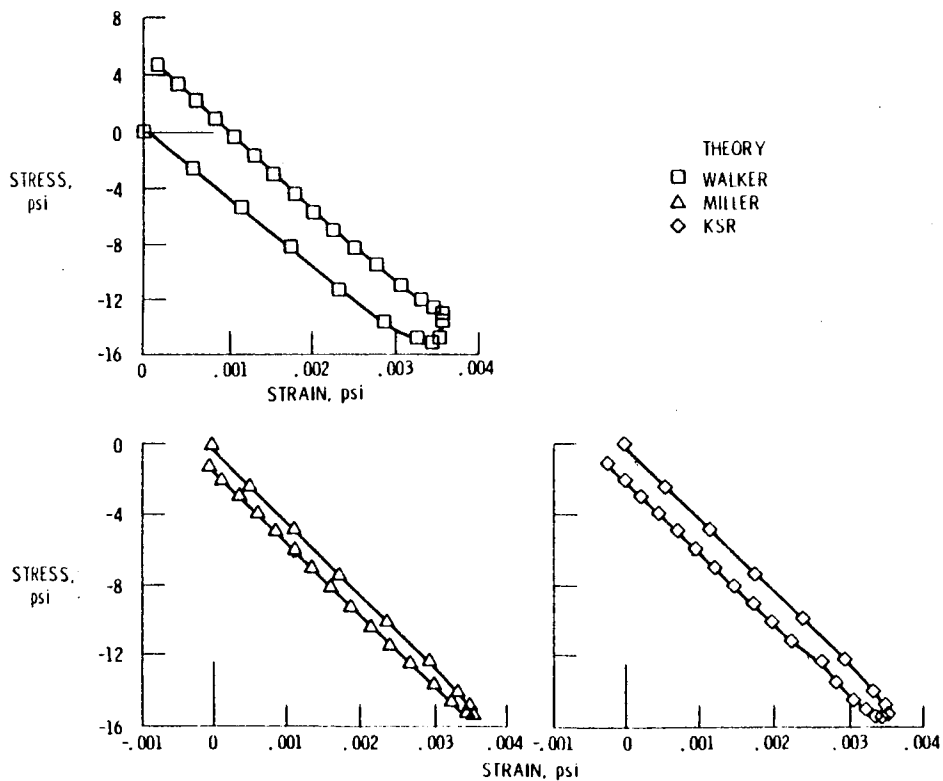


Figure 20